Research Article

Veprim Thaçi, Ramiz Hoti, Avni Berisha*, Jane Bogdanov*

Corrosion study of copper in aqueous sulfuric acid solution in the presence of (2*E*,5*E*)-2,5-dibenzylidenecyclopentanone and (2*E*,5*E*)-bis[(4-dimethylamino)benzylidene]cyclopentanone: Experimental and theoretical study

https://doi.org/10.1515/chem-2020-0172
received February 29, 2020; accepted August 25, 2020

Abstract: The corrosion behavior of copper in 0.1 M aqueous sulfuric acid medium has been studied using potentiodynamic polarization measurements, quantum chemical calculations, and molecular dynamic simulations in the presence and absence of (2*E*,5*E*)-2,5-dibenzylidenecyclopentanone (**M1**) and (2*E*,5*E*)-bis[(4-dimethylamino)benzylidene]cyclopentanone (**M2**). The compounds were freshly prepared in high yields via the Claisen–Schmidt reaction between the cyclopentanone and the corresponding aryl aldehyde. The results from the potentiodynamic measurements imply that **M1** and **M2** act as mixed inhibitors due to their adsorption on the copper surface. The more pronounced corrosion inhibition performance of the **M2** molecule in comparison to **M1** was related to the fact that this molecule contains two basic nitrogen atoms (in 4-dimethylamino group).

Keywords: copper corrosion, (2*E*,5*E*)-2,5-dibenzylidenecyclopentanone, (2*E*,5*E*)-bis[(4-dimethylamino)benzylidene]cyclopentanone, sulfuric acid medium, computational study

1 Introduction

Among the nonferrous metals, copper, due to its desirable properties, is among the most utilized. Even though it is known for its durability (in neutral aqueous systems), under certain conditions it is prone to corrosion [1,2]. Copper and its alloys are frequently used in different types of chemical equipment. In general, copper cannot displace hydrogen from acid solutions without the presence of dissolved oxygen [3]. However, most solutions contain dissolved air and are acidic. Corrosion inhibitors in many cases are employed to prevent copper corrosion. Control of copper corrosion is of immense technical, environmental, and economical importance. One simple and effective way to eliminate or slow down these processes is to use corrosion inhibitors [4–7]. Generally, the copper corrosion inhibitors are classified into inorganic and organic inhibitors. Lately, the organic inhibitors have been preferred and most of them are derivatives of benzotriazole [8,9]. However, serious environmental concerns have been raised over the extensive use of these types of additives, due to their persistence in sediments, resistance to degradation, and toxicity to aquatic organisms [10]. The quest for novel "green" copper corrosion inhibitors is ongoing.

Almost all of the relevant inhibitors are organic compounds containing one or more heteroatoms of which the most frequently encountered are nitrogen, oxygen, phosphorus, and sulfur. The corrosion protection performance exhibited by these organic compounds depends on the heteroatom present and usually decreases in the following order: O > N > S > P [11,12], but one has to be careful with such generalizations and take into consideration the functional group and steric factors. A vast number of molecules such as plant extracts, drugs, and synthetic organic molecules have been demonstrated to have good copper corrosion inhibition properties [13–18].

Many of the green renewable organic molecules, such as vanillin (plant-derived flavor compound) [15], caffeine [19], and other naturally occurring molecules,

* **Corresponding author: Avni Berisha,** Department of Chemistry, FNMS, University of Pristina "Hasan Prishtina", 10000 Pristina, Republic of Kosovo, e-mail: avni.berisha@uni-pr.edu
* **Corresponding author: Jane Bogdanov,** Department of Organic Chemistry, Institute of Chemistry, Faculty of Natural Sciences and Mathematics, Ss. Cyril and Methodius University, 1000 Skopje, Republic of Macedonia, e-mail: janebogdanov@gmail.com
Veprim Thaçi: Department of Chemistry, FNMS, University of Pristina "Hasan Prishtina", 10000 Pristina, Republic of Kosovo; Department of Organic Chemistry, Institute of Chemistry, Faculty of Natural Sciences and Mathematics, Ss. Cyril and Methodius University, 1000 Skopje, Republic of Macedonia
Ramiz Hoti: Department of Chemistry, FNMS, University of Pristina "Hasan Prishtina", 10000 Pristina, Republic of Kosovo

can be used as copper corrosion inhibitors. During our literature search for new potential copper corrosion inhibitors, we have encountered simple organic compounds with a unique electronic structure, so-called monocarbonyl analogs of curcumin (MACs). They have been extensively studied for their biological activity [20,21], but they have not been explored for corrosion inhibition of metals. The application of these MACs as corrosion inhibitors would broaden the range of compounds investigated and may lead to new insights into the mechanisms of the inhibitory action. After our investigation of the structural features of MACs based on the 2,5-diarylidenecyclopentanone core and following the cyclic voltammetry measurements, we have decided to explore their corrosion-inhibiting properties. The choice was to use the "parent" compound, (2*E*,5*E*)-2,5-dibenzylidenecyclopentanone (**M1**), and also the derivative with electron-donating dimethylamino substituent, (2*E*,5*E*)-bis[(4-dimethylamino)benzylidene]cyclopentanone (**M2**). Moreover, these kinds of derivatives are expected to be more eco-friendly than the benzotriazoles and related derivatives, because they are susceptible to *retro*-Claisen–Schmidt reaction and can revert back to the starting aldehyde and cyclopentanone, which are biodegradable. An additional useful feature is that **M2** is fluorescent [14–16] as a free amine and the fluorescence is quenched under acidic conditions (i.e., upon protonation of the dimethylamino group). These 2,5-diarylidenecyclopentanones are known compounds and their structure and properties have been thoroughly investigated (Scheme 1) [22–26].

These derivatives are synthetically accessible, their properties can be finetuned via synthesis, and finally they are not computationally demanding. Density functional theory (DFT) has become an expedient method to interpret experimental results, allowing the researcher to attain dependable structural parameters for molecules of various complexities [11,27,28]. This is also applicable to corrosion studies, where DFT allows accurate prediction of the inhibition efficiency (IE) of organic corrosion inhibitors on the basis of electronic and molecular properties as well as reactivity indexes [29]. Cost effectiveness is an important parameter when synthetic inhibitors are used [16]. The studied inhibitors suggested here offer the advantage of being synthesized in a single step using relatively inexpensive industrially available chemicals (cyclopentanone, benzaldehyde, and 4-(dimethylamino)benzaldehyde). Furthermore, if these compounds are promising, more derivatives can be easily synthesized and subjected to corrosion inhibition studies until the optimal derivative is found. In this study, two different compounds: (a) (2*E*,5*E*)-2,5-dibenzylidenecyclopentanone (**M1**) and (b) (2*E*,5*E*)-bis[(4-dimethylamino)benzylidene]cyclopentanone (**M2**) were used as corrosion inhibitors of copper in 0.1 M aqueous sulfuric acid medium. From the theoretical perspective, the adsorption mechanism and inhibition performance of **M1** and **M2** were surveyed as corrosion inhibitors by means of DFT at the B3LYP/6-31G (d,p) basis set level. Furthermore, molecular dynamics (MD) simulations were applied to calculate the adsorption geometries of the adsorbate, which was further explored by DFT with plane-wave basis set calculations to evaluate more precisely adsorption energies and the interaction with copper surface. Herein, we present the combined experimental and theoretical approach intended to gain insights into the potential of the 2,5-diarylidenecyclopentanones as copper corrosion inhibitors under acidic conditions.

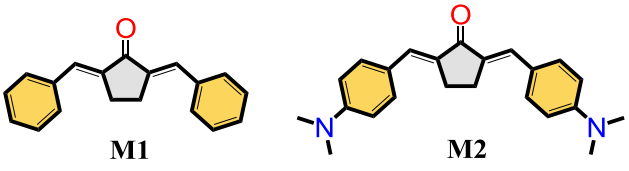

Scheme 1: Chemical structures of (2*E*,5E)-2,5-dibenzylidenecyclopentanone (**M1**) and (2*E*,5E)-bis[(4-dimethylamino)benzylidene] cyclopentanone (**M2**) inhibitors.

2 Materials and methods

2.1 Experimental section

2.1.1 Reagents and instruments

Cyclopentanone (99.8%), benzaldehyde (98%), and 4-(dimethylamino)benzaldehyde were obtained from Sigma-Aldrich. Methanol (99.9%, Chromasolv HPLC grade), dichloromethane, ethyl acetate, ammonium chloride, and sodium hydroxide were obtained from Merck. All the chemicals were used as received. Melting points were determined using Buchi B-545 melting-point apparatus. Infrared spectra were recorded on a Varian 3100 FTIR instrument by preparing solid samples as KBr pellets. ^{1}H and ^{13}C NMR spectra were obtained on a Bruker Avance 400 MHz spectrometer (at 400 and 100 MHz, respectively) in d_6-chloroform as a solvent and tetramethylsilane (TMS) as an internal standard. Chemical shifts were measured relative to TMS or the residual solvent in $CDCl_3$. The UV-Vis spectra were recorded on Helios Alpha Spectrophotometer on Cary 50 spectrophotometer in acetonitrile as a solvent.

For the potentiodynamic measurements, 97% sulfuric acid (Pro analysis; Merck, UN-No. 1830 Darmstadt, Germany) was used. This reagent was appropriately diluted with distilled water until a final concentration of

sulfuric acid of 0.1 mol/dm^3 was obtained, and this electrolyte was used throughout the electrochemical measurements. The electrode was made of commercial copper (d = 1 mm) wire. Before the electrochemical measurements, the copper surface was mechanically polished with emery paper, followed by cleaning with distilled water and then degreased in ethanol, washed with distilled water again, and air-dried. The linear sweep voltammetry (LSV) was performed using a PalSens3 potentiostat and applying a three-electrode cell assembly. A saturated calomel electrode (SCE) and a platinum electrode were used as reference and auxiliary electrodes, respectively. All solutions were prepared from analytic-grade chemicals and doubly distilled water. The copper electrode was allowed to stabilize its open circuit potential (OCP) until the potential stabilization met the criteria of dE/dt limit 10^{-6} V/s. Potentiodynamic polarization was carried out by scanning the potential ±500 mV from the evaluated OCP using a scan rate of 1 mV s^{-1}.

2.1.2 Synthesis of 2,5-diarylidenecyclopentanones

(2*E*,5*E*)-2,5-Dibenzylidenecyclopentanone (**M1**) was prepared by adaptation of the procedure described by Hadzi-Petrusev et al. [30]. Cyclopentanone (0.6309 g, 7.5 mmol) and benzaldehyde (1.5918 g, 15 mmol), followed by methanol (10 mL), were added in a round-bottomed flask (25 mL) equipped with a condenser. The solution was stirred at ambient temperature for 5 min; as a next step, a 20% (w/v) aqueous solution sodium hydroxide (2.0 mL) was added dropwise over a 5 min period. At first, the reaction mixture turned yellow and soon (after a few minutes) the yellow precipitate appeared. The reaction mixture was stirred for 45 min at ambient temperature. The reaction flask was lowered into an ice bath to be kept for 10 min, then 5 mL of water was added, and the content was filtered on a Büchner funnel. During the next stage, the yellow solid was washed with saturated aqueous ammonium chloride solution (1 × 10 mL), distilled water (3 × 10 mL), and ice-cold methanol (5 mL). The obtained yellow solid (1.68 g) was dried *in vacuo*. Recrystallization from hot methanol and dichloromethane gave 1.63 g (82%) of the desired product (**M1**) as yellow powder. m.p. 189–191°C (Lit. 196–198°C, [14]; 194–195°C [18]; 189–193°C [17]); ^{1}H NMR (400 MHz, $CDCl_3$) δ: 7.68–7.55 (m, 6H), 7.49–7.41 (m, 4H), 7.38 (dd, J = 8.4, 6.2 Hz, 2H), 3.13 (s, 4H). ^{13}C NMR (100 MHz, $CDCl_3$): δ 196.37 (C═O), 137.30, 135.83, 133.85, 130.73, 129.37, 128.76, 26.56. FT-IR (KBr): 1,692 cm^{-1} (m, C═O). UV-Vis (CH_3CN): λ_{max} = 354 nm.

(2*E*,5*E*)-2,5-Bis[(4-dimethylamino)benzylidene]cyclopentanone (**M2**) was prepared using the procedure outlined above using cyclopentanone (0.8412 g, 10 mmol) and 4-(dimethylamino)-benzaldehyde (2.9838 g, 20 mmol). Recrystallization from ethyl acetate gave 2.21 g (64%) of the desired product (**M2**) as orange powder. m.p. 302–304°C (Lit. 298°C, [14]; >300°C [16]). ^{1}H NMR (400 MHz, $CDCl_3$): δ 7.58–7.48 (m, 6H), 6.73 (d, J = 8.9 Hz, 4H), 3.07 (s, 4H), 3.03 (s, 12H). ^{13}C NMR (100 MHz, $CDCl_3$): δ 196.04 (C═O), 150.73, 133.52, 133.50, 132.54, 124.28, 111.89, 77.01, 76.70, 40.13, 26.66. FT-IR (KBr): 1,673 cm^{-1} (w, C═O). UV-Vis (CH_3CN): λ_{max} = 480 nm.

2.2 Computational details

2.2.1 DFT Calculations

DFT calculations were performed using Orca software [31,32]. The UV-Vis spectra and the rotation energy barrier for the studied molecules are computed using the DFT method by taking a relaxed geometry scan of 15 degree from 0° to 360° (25 energy calculations) along the dihedral angle presented in Section 3 using the B3LYP exchange–correlation density functional and the 6-31G** split-valence Pople basis sets.

2.2.2 Monte Carlo (MC) and MD simulations

MC and MD calculations were accomplished using Materials Studio 7.0 [33,34]. The interaction between iron surface and the inhibitor in the simulated corrosion media for MC is estimated by the slab model of Cu(11) with periodic boundary conditions (using a Cu unit cell, cleaved at the $h\,k\,l$ (1 1) plane and expanded to 10 × 10 with addition of an 30A vacuum layer at the C axis, containing 200 water molecules/one inhibitor molecule [either **M1** or **M2** molecule]/25 ethanol molecules and 60 hydronium + 30 sulfate ions). To assess the adsorption configurations (COMPASS II force field, energy convergence tolerance of 2 × 10^{-5} kcal/mol, force convergence tolerance of 0.001 kcal/mol/Å) and the interaction between the molecules and the substrates, the Metropolis Monte Carlo method was applied.

The MD simulations were performed using COMPASS II (Condensed-phase Optimized Molecular Potentials for Atomistic Simulation Studies) force field [35]. Prior to the use in the MD simulations, the slab model containing the corrosion media and the inhibitor molecule was optimized with the Smart optimization algorithm, whose energy convergence criteria were at the level of

10^{-4} kcal/mol and force criteria of 5×10^{-3} kcal/mol/Å. We use NVT (constant-temperature, constant-volume) canonical ensemble at 298 K to conduct MD. The time step for MD was 1 fs, and for the total simulation –500 ps. We controlled the system temperature with Berendsen Thermostat (0.1 ps decay constant) [36]. Furthermore, 500 ps of trajectory frames were used for the radial distribution function (RDF) analysis.

Ethical approval: The conducted research is not related to either human or animal use.

3 Results and discussion

3.1 Linear polarization

The compounds (2*E*,5*E*)-2,5-dibenzylidenecyclopentanone (**M1**) and (2*E*,5*E*)-bis[(4-dimethylamino)benzylidene]cyclopentanone (**M2**) were freshly prepared via the Claisen–S chmidt reaction between the cyclopentanone and corresponding aryl aldehyde in 82 and 64% yields, respectively. They are known compounds (dienones) with *E*, *E* stereochemistry and their spectroscopic data match those reported in the literature [22,25].

The polarization plots obtained for the copper electrode in a 0.1 M sulfuric acid aqueous solution in the presence and the absence of **M1** and **M2** are presented in Figure 1. Potentiodynamic measurements for the Cu electrode showed a fast increase of the anodic current, after the corrosion potential. This is due to an active dissolution of copper at a slightly positive potential, around 0.08 V. The inhibition behavior of both the studied molecules (**M1** and **M2**) is evidenced by the decreased cathodic current densities. The cathodic and anodic Tafel slopes and corrosion potential (E_{corr}), kinetic electrochemical corrosion parameters, and corrosion current density (I_{corr}) were calculated from the extrapolation of Tafel plots (values in Table 1).

Albeit the corrosion current density decreases in the presence of **M1** and **M2**, there is no apparent corrosion potential change significantly in the presence of these inhibitor molecules. The cathodic Tafel slope is larger than that of the anodic one, and the corrosion potential is slightly displaced cathodically, showing that the protective barrier formed from the adsorbed molecules acts mainly as a cathodic inhibitor. We calculated the IE using the corrosion current density of the metal electrodes in the absence and presence of the inhibitor, with the following equation:

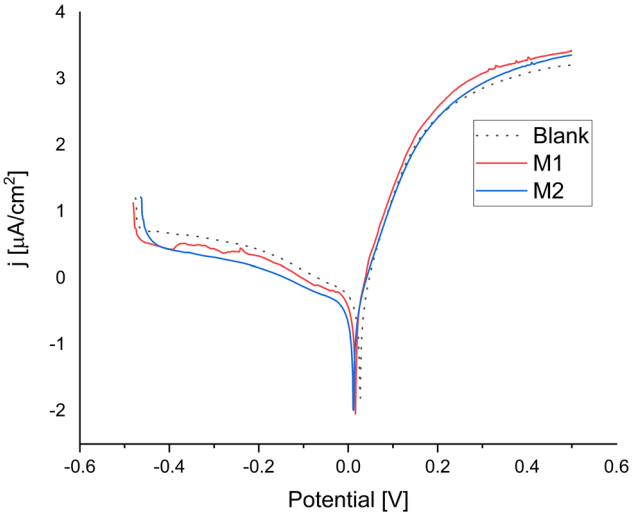

Figure 1: Semilogarithmic polarization plots of the copper electrode in a 0.1 M H_2SO_4 (70:30 water:ethanol) aqueous solution with and without the presence of 0.001 mol/dm^3: **M1** and (b) **M2**. Reference SCE. $v = 1$ mV/s.

Table 1: Results of Tafel slope analysis of the polarization plots at 298 K

Corrosion parameters	Blank	M1	M2
E corrosion (V)	–0.023	–0.067	0.004
j corrosion d (A/cm²)	1.195	1.026	0.468
Polarization Resistance (Ω)	2.86×10^4	3.68×10^4	5.09×10^4
Anodic β Tafel constant (V/decade)	0.091	0.104	0.063
Cathodic β Tafel constant (V/decade)	0.564	0.537	0.445
Corrosion rate (mm/year)	0.441	0.378	0.173
IE (%)	—	14.142	60.840

$$\text{IE}\ (\%) = (I_{\text{unhib.}}) - (I_{\text{inh.}})/(I_{\text{unhib.}}) \times 100.$$

The calculated IEs for **M1** and **M2** were 14.1 and 60.8%, respectively, and the corrosion rates were 0.378 mm/year and 0.173 mm/year, respectively.

3.2 UV-Vis spectroscopy

To fully understand the copper corrosion inhibition behavior of these derivatives, which have a unique π-conjugated structure, information on both the ground-state and excited-state structures and the frontier molecular orbitals was helpful. This was a preliminary study to see what are the changes upon electronic excitation. Both **M1** and **M2** are colored in the solid state and solution (yellow and bright

orange, respectively). The UV-Vis spectra were recorded in acetonitrile (200–800 nm) and **M1** and **M2** had absorption maxima at 354 and 480 nm, respectively. Both compounds have relatively high molar extinction coefficients (ε): $\varepsilon_{(\mathbf{M1})}$ = 15,983 $M^{-1}\,cm^{-1}$ and $\varepsilon_{(\mathbf{M2})}$ = 6,99,24 $M^{-1}\,cm^{-1}$. **M2** is also fluorescent and the fluorescence is solvent dependent. This may be a useful feature to further explore the effects of electronic excitation on the adsorption of **M1** or **M2** on the copper surface (Figure 2).

To provide molecular insights into the UV-Vis absorption of these compounds, we performed an investigation based on the TDDFT method. The plots of computational data are presented in Figure 3. The computed UV-Vis spectra show similarities with the experimental one.

The isosurface plots for the natural transition orbitals (NTOs), involved in the electronic transition responsible for the UV-Vis absorptions, are depicted in Figure 3 (insets on the UV-Vis spectra). Distributions of NTOs for the transition state at lower wavenumbers are mainly from benzene rings toward the central cyclopentanone moiety. The absorption at the higher wavelengths is electronic transition from the π system of the aromatic side rings to the double bond that links the phenyl ring with the central cyclopentanone ring. The electronic transitions are consistent with those expected for dibenzylidenecyclopentanone compounds, exhibiting π → π* transition at a lower wavelength and n → π* at higher ones.

3.3 Rotation energy barrier

The dihedral scan from 0 to 360 degree using a 15-degree step scan for both the molecules in the gas phase is

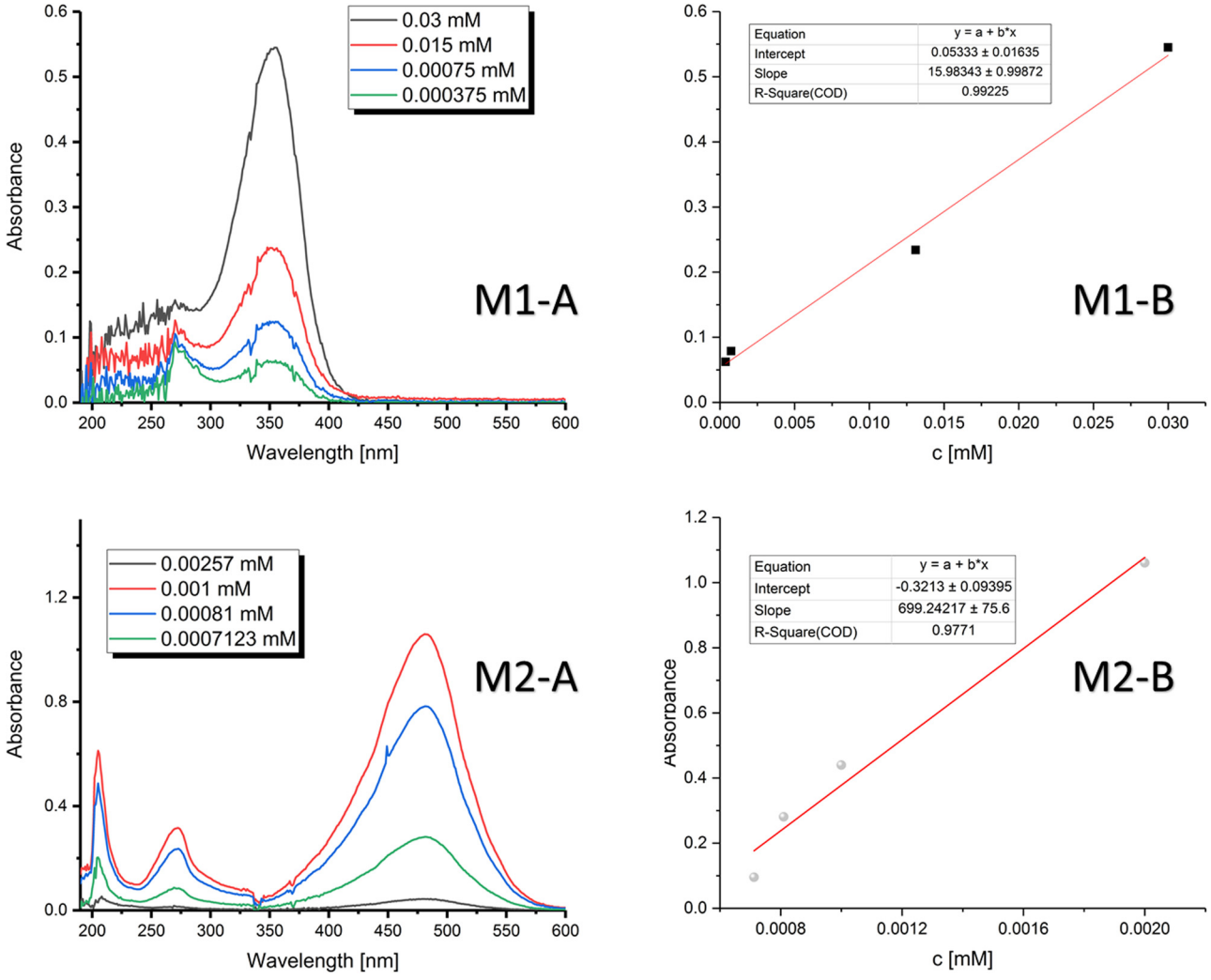

Figure 2: UV-Vis spectra of **M1** (top left) and **M2** (bottom left) in acetonitrile. Plots for determination of the extinction coefficients for **M1** (top right) and **M2** (bottom right).

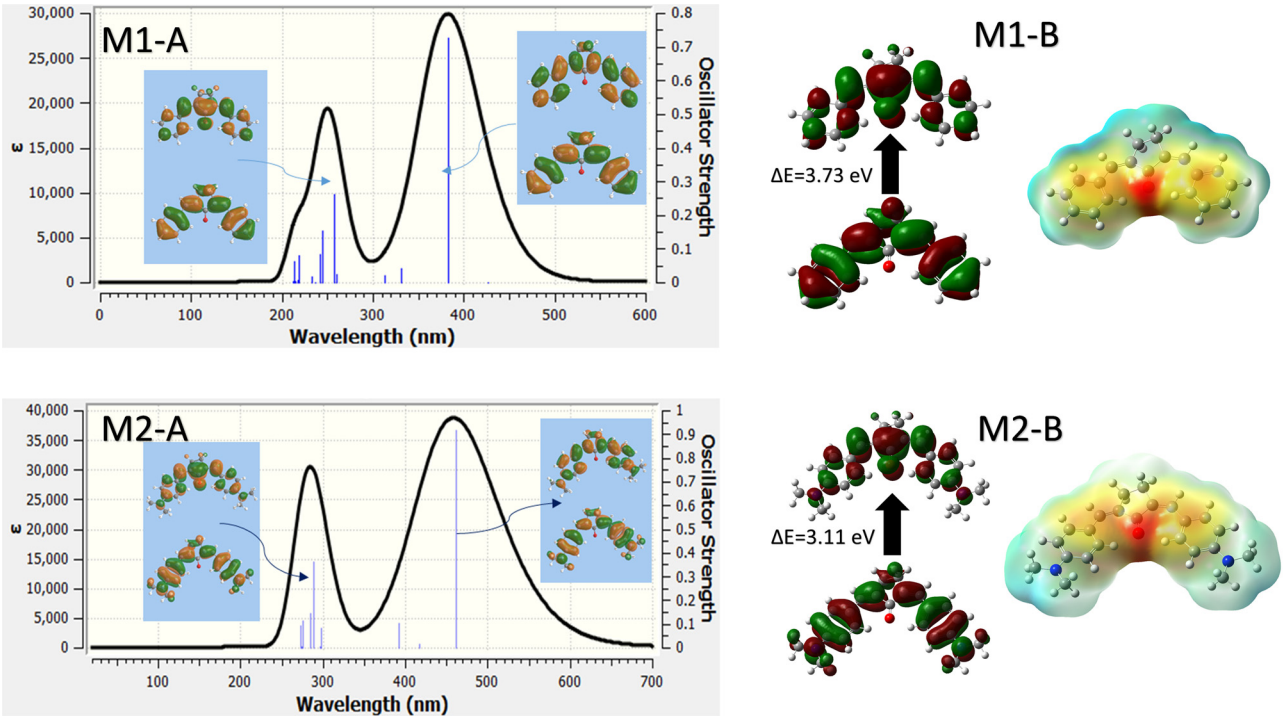

Figure 3: Calculated UV-Vis spectra of **M1** (top left) and **M2** (bottom left) in acetonitrile. Frontier molecular orbitals relevant for the electronic transition and the corresponding energy differences – **M1** (top right) and **M2** (bottom right).

presented in Figure 4. The required energy for complete rotation is 48.39 kcal/mol for **M1** and 52.91 kcal/mol for **M2**.

The rotation barrier of the molecules is in the same range as the stilbene molecules (48.3 kcal/mol).

3.4 MC calculations

Figure 5 shows the distribution of the adsorption energies during the MC calculations for the species used to simulate the corrosion media. Being dependent on configuration of inhibitor onto the Cu surface for **M1** molecule, adsorption energy shows the results within the range of −25.44 to −45.45 kcal/mol, whereas the adsorption energy for the **M2** is in the range of −88.55 to −117.75 kcal/mol. The negative energy values are an indication of spontaneity of the inhibitor adsorption toward the copper surface.

These rather high adsorption energy values are considered to be responsible for the water displacement from the Cu(111) surface caused by the interaction of the inhibitor by electron sharing of their oxygen (**M1** and **M2**) and nitrogen (for **M2**) and the surface. This involves the overlap between the sharing of electrons from –O and –N atoms of the inhibitor and the 3d electrons of the copper surface [37].

3.5 MD

Intending to recognize the interaction details of the studied inhibitor with the Cu(110) surface at the molecular level, the MD simulations were performed. The most stable geometry configurations (Figure 6), together with the RDF poses (Figure 7) acquired from these

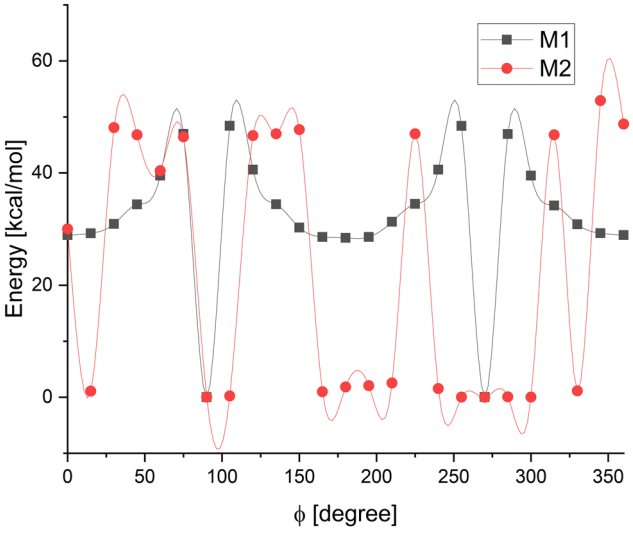

Figure 4: Calculated rotational energy barrier (gas phase) for **M1** (black trace) and **M2** (red trace).

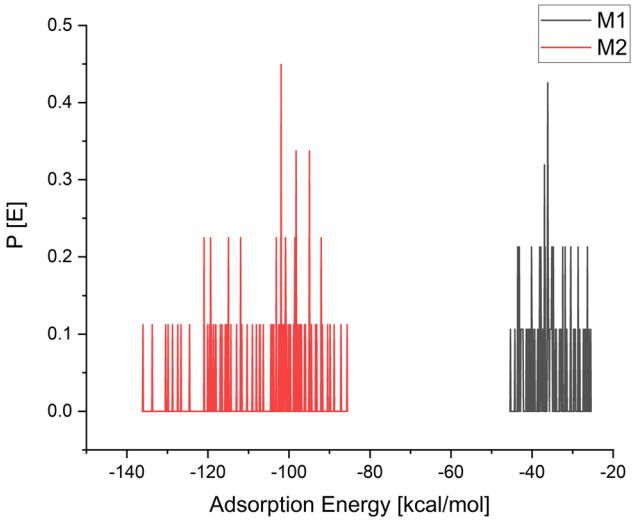

Figure 5: Probability of adsorption energy distribution curves for Cu (111)/**M1** or **M2** + 200 water molecules/one inhibitor molecule (either **M1** or **M2** molecule)/25 ethanol molecules and 60 hydronium +30 sulfate-simulated corrosion media obtained via MC calculations.

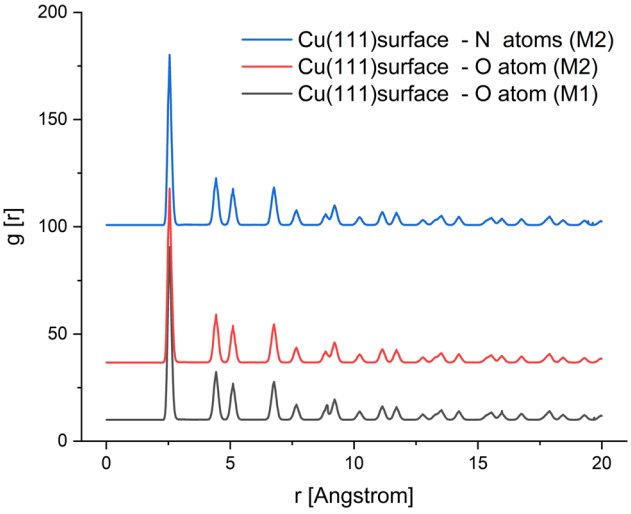

Figure 7: RDF of O and N atoms of **M1** and **M2** inhibitor molecules on the Cu(111) surface.

simulations, delivered an in-depth data concerning the corrosion inhibition expressed by these two molecules.

Both the studied inhibitors are flat lying onto the copper surface, and the higher value of adsorption energy (from MC) in the case of **M2** compared to **M1** is due to a greater surface and the presence of two additional nitrogen atoms of the former one.

The RDF is often used in MD simulations to assess the interaction type between the studied inhibitors and the surface. When the peaks reach the distances from 1 Å up to 3.5 Å, it is considered as a sign associated normally with the chemisorption (for the physisorption the peaks start at the distances bigger than 3.5 Å) [38]. The RDF value (Figure 7) for O atom of both molecules shows that the bond length of O atoms and the copper surface is less than 3.5 Å, directing to chemisorption of the inhibitors. This strong interaction causes metal protection against dissolution – through a chemisorption process.

3.6 Adsorption and corrosion inhibition mechanism of M1 and M2 inhibitors

The inhibition performance of an inhibitor is related to its adsorption ability on the interface of the metal. This adsorptive interaction led to the formation of a protective layer onto the metal surface that protects the metal from corrosion [40] From the obtained experimental and theoretical results, the following adsorption mechanism is proposed (Figure 8).

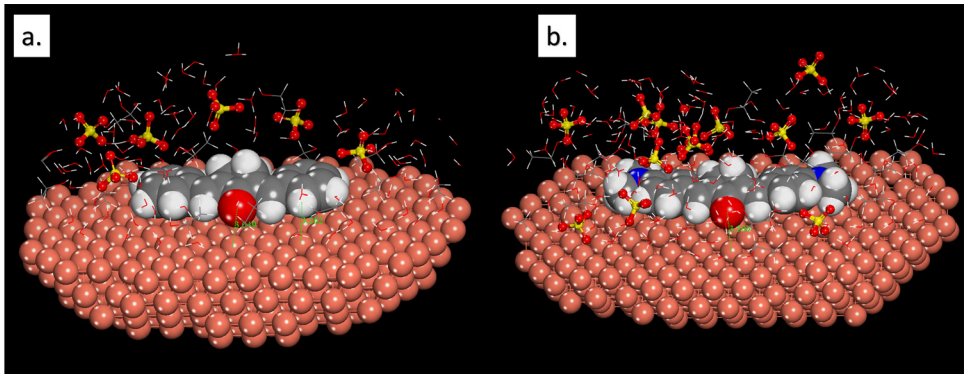

Figure 6: Views of the most stable adsorption configuration for Cu (111)/(a) **M1** or (b) **M2** (b)/25 ethanol molecules and 60 hydronium + 30 sulfate-simulated corrosion media obtained via MD simulations.

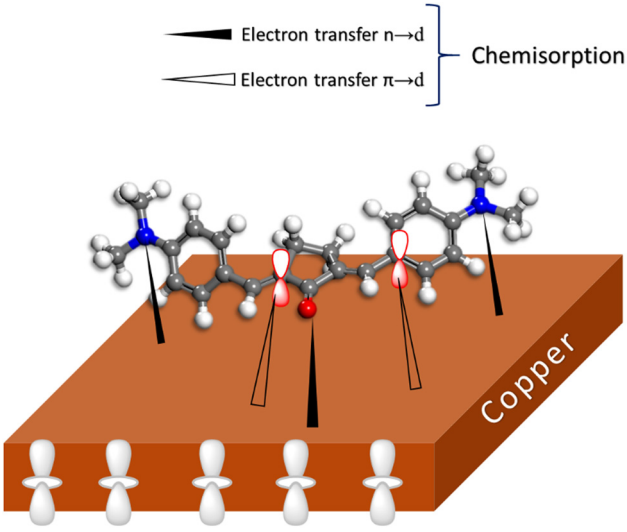

Figure 8: The proposed adsorption mechanism of the **M2** inhibitor on the copper surface.

Monocurcumin molecules were chemically adsorbed onto the Cu surface by donor/acceptor interaction between free electron pairs of heteroatoms (oxygen for **M1**; oxygen and nitrogen for the **M2**) and the vacant d-orbital of the copper surface [39]. A crucial role for the adsorptive interaction is also the donor/acceptor interaction between the antibonding molecular orbitals of curcumin inhibitors and the d-orbitals of the copper atoms of the surface [40].

4 Conclusions

The corrosion behavior of copper in 0.1 M aqueous sulfuric acid medium was investigated using potentiodynamic polarization measurements, quantum chemical calculations, and MD simulations in the presence and absence of (2*E*,5*E*)-2,5-dibenzylidenecyclopentanone (**M1**) and (2*E*,5*E*)-bis[(4-dimethylamino)benzylidene]cyclopentanone (**M2**). The main electronic transitions in the studied compound as supported by TDFT calculations $\pi \rightarrow \pi^*$ transition at a lower wavelength and $n \rightarrow \pi^*$ at higher ones. MD results show that these molecules are flat adsorbed onto the copper surface. Selecting suitable substituents on the dibenzylidenecyclopentanone system as shown here led to different corrosion inhibition performance. In our ongoing studies, we have been exploring these effects. The more pronounced corrosion inhibition performance of the **M2** derivative in comparison to **M1** was related to the fact that this molecule contains two basic nitrogen atoms (in 4-dimethylamino group). These nitrogen atoms increase the adsorption ability of this molecule as found from theoretical calculations.

Acknowledgments: The authors gratefully acknowledge the support from the Ministry of Education, Science and Technology of Kosovo (No. 2-5069) for providing him with the computing resources.

Conflict of interest: The authors declare no conflict of interest.

References

[1] Schutze M, Feser R, Bender R. Corrosion resistance of copper and copper alloys. Morlenbach. Germany: Wiley-VCH; 2011.
[2] Zhou P, Ogle K, Wandelt K. The corrosion of copper and copper alloys. In Encyclopedia of Interfacial Chemistry. Oxford, UK: Elsevier; 2018. p. 478–89.
[3] Telegdi J, Shaban A, Kálmán E. EQCM study of copper and iron corrosion inhibition in presence of organic inhibitors and biocides. Electrochim Acta. 2000;45(22–23):3639–47.
[4] Antonijević MM, Petrović MB. Copper corrosion inhibitors. A Review. Int J Electrochem Sci. 2008;3:1–28.
[5] Raja PB, Ismail M, Ghoreishiamiri S, Mirza J, Ismail M, Kakooei S, et al. Reviews on corrosion inhibitors: A short view. Chem En Commun. 2012;203:1145–56.
[6] Petrović Mihajlović MB, Antonijević MM. Copper corrosion inhibitors. Period 2008–2014. A Review. Int J Electrochem Sci. 2015;10:1027–53.
[7] Fateh A, Aliofkhazraei M, Rezvanian AR. Review of corrosive environments for copper and its corrosion inhibitors. Arab J Chem. 2020;13:481–544.
[8] Walker R. Triazole, benzotriazole and naphthotriazole as corrosion inhibitors for copper. Corros. 1975;31:97–100.
[9] Finšgar M, Milošev I. Inhibition of copper corrosion by 1,2,3-benzotriazole: A review. Corros Sci. 2010;52:2737–49.
[10] Cantwell MG, Sullivan JC, Burgess RM, Zeng EY. Chapter 16-benzotriazoles: History, environmental distribution, and potential ecological effects. In Comprehensive Analytical Chemistry. Elsevier; 2015. p. 513–45.
[11] Berisha A, Podvorica F, Mehmeti V, Syla F, Vataj D. Theoretical and experimental studies of the corrosion behavior of some thiazole derivatives toward mild steel in sulfuric acid media. Maced J Chem Chem En. 2015;34:287–94.
[12] Mohsenifar F, Jafari H, Sayin K. Investigation of thermodynamic parameters for steel corrosion in acidic solution in the presence of *N*,*N*-bis(phloroacetophenone)-1,2-propanediamine. J Bio Tribo Corros. 2016;2:1–13.
[13] Popoola LT. Organic green corrosion inhibitors (OGCIs): A critical review. Corros Rev. 2019;37(2):71–102.
[14] Rani BEA, Basu BBJ. Green inhibitors for corrosion protection of metals and alloys: An overview. 2012;15:380217. doi: 10.1155/2012/380217

[15] Mo Sh LiLJ, Luo HQ, Li NB. An example of green copper corrosion inhibitors derived from flavor and medicine: vanillin and isoniazid. J Mol Liq. 2017;242:822–30.
[16] Tan J, Guo L, Yang H, Zhangc F, Bakri YE. Synergistic effect of potassium iodide and sodium dodecyl sulfonate on the corrosion inhibition of carbon steel in HCl medium: a combined experimental and theoretical investigation. RSC Adv. 2020;10:15163–70.
[17] About S, Zouarhi M, Chebabe D, Damej M, Berisha A. Najat Hajjaji. Galactomannan as a new bio-sourced corrosion inhibitor for iron in acidic media. Helyon. 2020;6:03574.
[18] Rbaa M, Dohare P, Berisha A, Dagdag O, Lakhrissi L, Galai M, et al. New epoxy sugar based glucose derivatives as eco friendly corrosion inhibitors for the carbon steel in 1.0 M HCl: Experimental and theoretical investigations. J Alloy Compd. 2020;833:154949.
[19] Souza FS, Giacomelli C, Gonçalves RS, Spinellia A. Adsorption behavior of caffeine as a green corrosion inhibitor for copper. Mater Sci Eng C. 2012;32(8):2436–44.
[20] Zhao C, Liu Z, Liang G. Promising curcumin-based drug design: Mono-carbonyl analogues of curcumin (MACs). Cur Pharm Des. 2013;19:2114–2135.
[21] Shetty D, Kim JY, Shim H, Snyder PJ. Eliminating the heart from the curcumin molecule: Monocarbonyl curcumin mimics (MACs). Molecules. 2015;20:249–92.
[22] Vatsadze SZ, Gavrilova GV, Zyuz'kevich FS, Nuriev VN, Krut'ko DP, Moiseeva AA, et al. Synthesis, structure, electrochemistry, and photophysics of 2,5-dibenzylidenecyclopentanones containing in benzene rings substituents different in polarity. Russ Chem Bull. 2016;65:1761–72.
[23] Zakharova GV, Zyuz'kevich FS, Gutrov VN, Gavrilova GV, Nuriev VN, Vatsadze SZ, et al. Effect of substituents on spectral, luminescent and time-resolved characteristics of 2,5-diarylidene derivatives of cyclopentanone. High Energy Chem. 2017;51:113–7.
[24] Li Z, Pucher N, Cicha K, Torgersen J, Ligon SC, Ajami A, et al. A straightforward synthesis and structure-activity relationship of highly efficient initiators for two-photon polymerization. Macromolecules. 2013;46:352–61.
[25] Carapina da Silva C, Pacheco BS, das Neves RN, Dié Alves MS, Sena-Lopes A, Moura S, et al. Antiparasitic activity of synthetic curcumin monocarbonyl analogues against *Trichomonas vaginalis*. Biomed Pharmacother. 2019;111:367–77.
[26] Leow P-C, Bahety P, Boon CP, Lee CY, Tan KL, Yang T, et al. Functionalized curcumin analogs as potent modulators of the Wnt/beta-catenin signaling pathway. Eur J Med Chem. 2014;71:67–80.
[27] Geerlings P, DeProft F, Langenaeker W. Conceptual density functional theory. Chem Rev. 2003;103:1793–874.
[28] Gece G. The use of quantum chemical methods in corrosion inhibitor studies. Corros Sci. 2008;50:2981–92.
[29] Obot IB, Macdonald DD, Gasem ZM. Density functional theory (DFT) as a powerful tool for designing new organic corrosion inhibitors. Part 1: An overview. Corros Sci. 2015;99:1–30.
[30] Hadzi-Petrushev N, Bogdanov J, Krajoska J, Ilievska J, Bogdanova-Popov B, Gjorgievska E, et al. Comparative study of the antioxidant properties of monocarbonyl curcumin analogues C_{66} and B_2BrBC in isoproteranol induced cardiac damage. Life Sci. 2018;197:10–8.
[31] Neese F. The ORCA Program System. WIREs Comput Mol Sci. 2012;2:73–8.
[32] Neese F. Software Update: the ORCA Program System, version 4.0. WIREs Comput Mol Sci. 2018;8:e1327.
[33] Akkermans RLC, Spenley NA, Robertson SH. Monte Carlo methods in materials studio. Mol Simulat. 2013;39:1153–64.
[34] Mehmeti VV, Berisha AR. Corrosion study of mild steel in aqueous sulfuric acid solution using 4-methyl-4*H*-1,2,4-triazole-3-thiol and 2-mercaptonicotinic acid – an experimental and theoretical study. Front Chem. 2017;5:61. doi: 10.3389/fchem.2017.00061.
[35] Sun H, Jin Z, Yang C, Akkermans RLC, Robertson SH, Spenley NA, et al. COMPASS II: extended coverage for polymer and drug-like molecule databases. J Mol Model. 2016;22(2):47.
[36] Lemak AS, Balabaev NK. On the Berendsen Thermostat. Mol Simul. 1994;13:177–87.
[37] Hsissou R, Abbout S, Berisha A, Berradi M, Assouag M, Hajjaji N, et al. Experimental, DFT and molecular dynamics simulation on the inhibition performance of the DGDCBA epoxy polymer against the corrosion of the E24 carbon steel in 1.0 M HCl solution. J Mol Struct. 2019;1182:340–51.
[38] Tan J, Guo L, Lv T, Zhang S. Experimental and computational evaluation of 3-indolebutyric acid as a corrosion inhibitor for mild steel in sulfuric acid solution. Int J Electrochem Sci. 2015;10:823–87.
[39] Berisha A. Experimental, Monte Carlo and molecular dynamic study on corrosion inhibition of mild steel by pyridine derivatives in aqueous perchloric acid. Electrochem. 2020;1(2):188–99.
[40] Lgaz H, Bhat KS, Salghi R, Jodeh S, Shubhalaxmi, Algarra M, et al. Insights into corrosion inhibition behavior of three chalcone derivatives for mild steel in hydrochloric acid solution. J Mol Liq. 2017;238:71–83.